Composites Part B 274 (2024) 111257

Contents lists available at ScienceDirect

Composites Part B

journal homepage: www.elsevier.com/locate/compositesb

Thermal-, magnetic-, and light-responsive 4D printed SMP composites with multiple shape memory effects and their promising applications

Cheng Lin [a,1], Xiaozhou Xin [b,1], Linfeng Tian [a], Dou Zhang [b], Liwu Liu [b,**], Yanju Liu [b,*], Jinsong Leng [a]

[a] Centre for Composite Materials and Structures, Harbin Institute of Technology, No. 2 Yikuang Street, Harbin, 150001, PR China
[b] Department of Astronautical Science and Mechanics, Harbin Institute of Technology, No. 92 West Dazhi Street, Harbin, 150001, PR China

ARTICLE INFO

Handling Editor: Dr Hao Wang

Keywords:
Multi-responsive
4D printing
Multi-shape memory polymers
Selective actuation
Programmability

ABSTRACT

Driven by increasingly complex functional requirements, the shape memory polymer (SMP) is more competitive due to its convertible configuration and tunable properties. In particular, the multi-shape SMP that is not limited to one temporary configuration gives more possibilities for intelligent applications of SMP. However, it is still challenging to manufacture highly controllable and selectively programmable multi-shape SMP in a facile and scalable manner. Here, thermal-, magnetic-, and light-responsive 4D printed SMP composites with up to eight shape memory effects were developed, with the advantages of selective programming, highly controllable deformation in time and space, and configuration customization. The introduction of 4D printing into the manufacturing of multi-responsive SMP composites allowed for easy implementation and rapid manufacturing of controllable and customizable dynamic structures. Through the design of multi-material and multi-structural modules, coupled with 4D printing technology, the multi-responsive SMP composites were endowed with unlimited design freedom. 4D printed multi-responsive SMP composites realized accurate and selective actuation, tripled programmability, and efficient encrypted transmission of multiple types of information (e.g., encrypted transmission of idioms in the form of combined graphs and text), showing attractive application prospects in flexible robots, highly programmed metamaterials, information encryption carriers, etc.

1. Introduction

Shape memory polymers (SMPs) are a class of stimuli-responsive materials that possess the ability to program to temporary configurations and recover to a predefined initial configuration upon stimuli such as heat, light, water/humidity, electric and magnetic fields [1,2]. The extraordinary configuration transformation capability of SMP endows it with progressiveness in structure and performance, showing broad application potential in many fields, such as aerospace, textile manufacturing, flexible electronics, soft robotics, biomedicine, etc. [2–5].

Despite extensive work on autonomous transformation configurations for SMPs, it remains a challenge to achieve selectively programmable deformations that are highly controllable in time and space [6]. Typically, SMPs are limited to switching between two configurations (dual shape memory effect), which means that SMPs can only be programmed to a single temporary configuration and then recover to the initial/permanent configuration during a shape memory cycle. To increase programming flexibility to accommodate applications requiring more tunable configurations, SMPs with multiple shape memory effects that can remember more than two temporary configurations are developed, among which triple-shape SMP is the most common multi-shape SMP. Triple-shape SMP can be obtained by broadening the shape memory transition region or by integrating phases with discrete transition temperatures into a single SMP. Implementation strategies include the preparation of interpenetrating polymer networks, copolymerization, grafting, etc. [7–13]. However, to obtain different temporary configurations in one shape memory cycle, the transition temperature interval of the two temporary configurations in triple-shape SMP is usually required to be more than 20 °C. Otherwise, the temporary configurations will interfere with each other, resulting in unsatisfactory shape fixation/recovery performance. Such a wide temperature range is

* Corresponding author.
** Corresponding author.
E-mail addresses: liulw@hit.edu.cn (L. Liu), yj_liu@hit.edu.cn (Y. Liu).
[1] These authors contributed equally.

https://doi.org/10.1016/j.compositesb.2024.111257
Received 6 September 2023; Received in revised form 23 January 2024; Accepted 27 January 2024
Available online 2 February 2024
1359-8368/

impractical in many applications, such as textile products, biomedical devices, etc. More importantly, achieving a controlled range and several transition temperatures in SMP is extremely inefficient, and the cumbersome and time-consuming molecular design and synthetic preparation routes greatly limit the feasibility of further practical applications of the synthesized SMPs. In addition, the most widely explored SMPs typically accomplish shape recovery in a holistic manner through thermal or other actuation methods (e.g., light, magnetic fields, humidity), which severely hinders the requirement for selective programmed actuation of preset regions. Therefore, it is of great significance to develop an easy-to-implement, economical, rapid, and scalable manufacturing strategy to obtain multi-shape SMPs with highly controllable and selectively programmable deformability to serve real-world practical applications.

3D printing is capable of creating highly complex structures in a large-scale and rapid manner, breathing new life into the manufacturing industry [14–18]. However, 3D printed structures are static, greatly limiting the applications that require dynamic reshaping of the configuration. This limitation can be perfectly addressed by preparing SMPs as printable raw materials and combining them with 3D printing, which gives rise to 4D printing. 4D printing adds time as an additional dimension to 3D printing, enabling 3D printed structures to dynamically deform in response to environmental stimuli [19–24]. Due to the integration of the strengths of 3D printing and SMP, 4D printing has shown unique advantages in electronic devices, intelligent soft robots, biomedicine, self-assembled structures, etc. [25–29].

Here, a facile strategy was proposed to fabricate 4D printed SMP composites with multiple shape memory effects, capable of responding to thermal, magnetic fields, and light. Since compounding functional fillers into the polymer matrix in a blended manner is an efficient and easy-to-process method, it avoids the obstacles to large-scale production caused by cumbersome synthetic routes. Therefore, by introducing Fe_3O_4 nanoparticles and multi-walled carbon nanotubes (MWCNTs) functional fillers into the shape memory polylactic acid (SMPLA) matrix, the magnetic and light responsiveness of 4D printed SMP was achieved (Fig. 1). The magnetic- and light-responsive SMP composites showed excellent magneto-thermal and photothermal properties and demonstrated outstanding shape memory performance. Thermal-, magnetic-, and light-responsive 4D printing filaments capable of scalable production were prepared, clearing the way for the practical application of functional devices. 4D printed SMP composites enabled selective, controlled, and precise actuation, showing attractive applications in flexible robotics, highly programmable metamaterials, and information encryption carriers.

2. Results and discussion

2.1. Characterizations

The tensile properties of SMPLA, Mag-SMPLA, and Lig-SMPLA at different temperatures were evaluated. Among them, the tensile strength of Mag-SMPLA was slightly lower than that of SMPLA but slightly higher than that of Lig-SMPLA (Fig. 2a–d). The tensile strength decreased with increasing temperature. At 25 °C, the tensile strengths of SMPLA, Mag-SMPLA, and Lig-SMPLA were 45.87 MPa, 40.73 MPa, and 38.00 MPa. At 35 °C, the tensile strengths of SMPLA, Mag-SMPLA, and Lig-SMPLA were 37.44 MPa, 36.90 MPa, and 35.14 MPa, respectively. The elongation at break increased sharply with the increase of temperature (Fig. 2a–c, Table S1). At 45 °C the elongation at break of SMPLA was significantly higher than that of Mag-SMPLA and Lig-SMPLA. This may be because the magnetic nanoparticles and MWCNTs hindered the movement of the matrix chain segments and delayed the temperature at which the chain segments initiated large-amplitude motion. At 55 °C, the elongation at break of Mag-SMPLA and Lig-SMPLA also increased significantly, rising to 274.00 % and 197.72 %, respectively. At this temperature, the typical characteristics of yielding, strain softening, plastic deformation, and strain hardening of the specimens were shown, and the macroscopic "thin neck" phenomenon also appeared obviously (Fig. S1). As the temperature was close to their T_g, the yield phase of SMPLA, Mag SMPLA, and Lig-SMPLA became less pronounced when the temperature rose to 65 °C. The bending properties were evaluated by three-point bending tests. The elongation at break of Mag-SMPLA and Lig-SMPLA was significantly higher than that of SMPLA, and the flexural strengths of the three were close (Fig. 2e). The thermal behavior of Mag-SMPLA and Lig-SMPLA was investigated (Fig. 2f). Since the thermal behavior of SMPLA has been studied in detail in our previous work [20], there was no redundant repetition here. The glass transition temperature (T_g) and melting temperature (T_m) of SMPLA, Mag-SMPLA, and

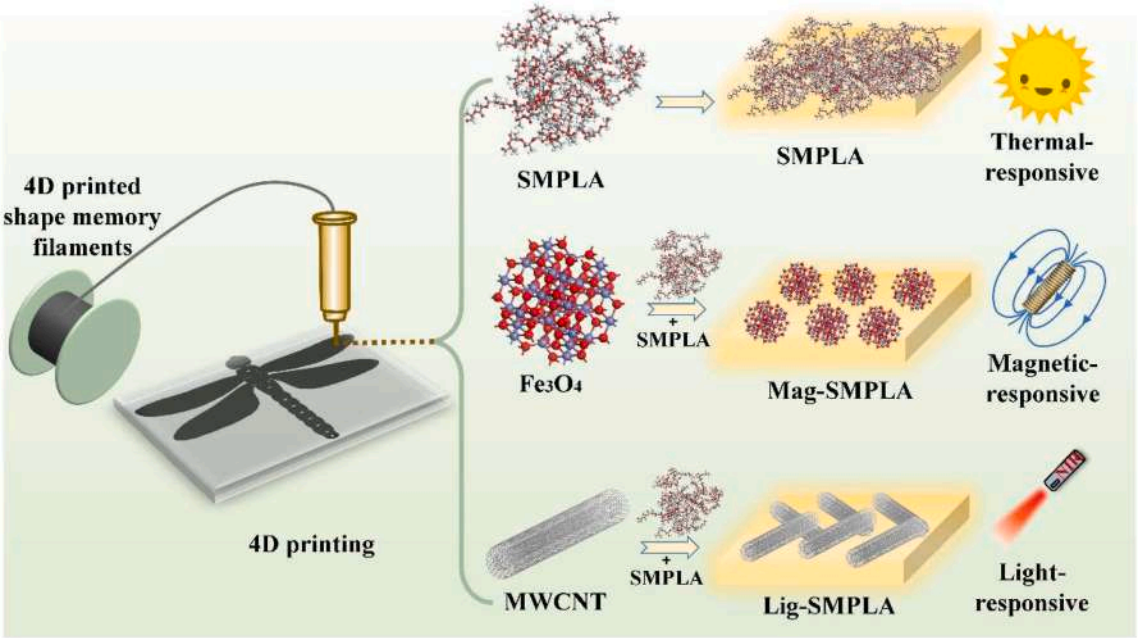

Fig. 1. Thermal-, magnetic-, and light-responsive 4D printed SMPLA filaments. "Mag-SMPLA" represents the 4D printed magnetic-responsive SMPLA. "Lig-SMPLA" represents the 4D printed light-responsive SMPLA.

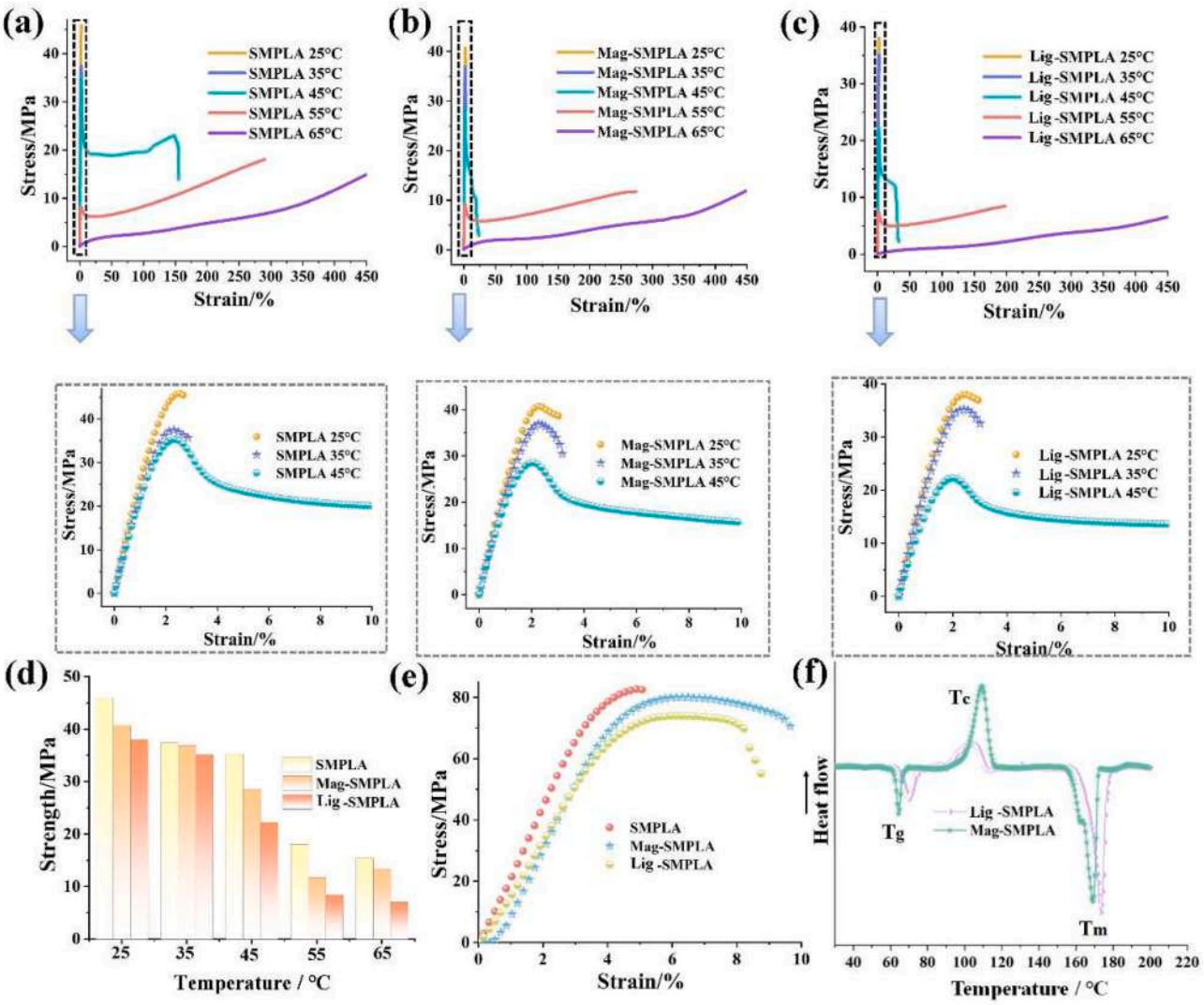

Fig. 2. Mechanical properties of SMPLA, Mag-SMPLA, and Lig-SMPLA. Tensile tests of (a) SMPLA, (b) Mag-SMPLA, and (c) Lig-SMPLA at different temperatures. The second row is enlarged views of the tensile test curves. (d) Tensile strength. (e) Three-point bending tests at room temperature. (f) Differential scanning calorimetry (DSC) tests. T_g: glass transition temperature; T_c: crystallization temperature; T_m: melting temperature.

Lig-SMPLA were very close, with T_g approximately 66 ± 3 °C and T_m approximately 170 ± 3 °C. The cold crystallization temperatures (T_c) of Mag-SMPLA and Lig-SMPLA were shifted to lower temperatures compared to SMPLA, which may be due to the fact that magnetic nanoparticles and MWCNTs acted as nucleation sites and thus promoted the crystallization of the matrix.

The deformation repeatability of SMPLA, Mag-SMPLA, and Lig-SMPLA was evaluated by loading-unloading cycles (Fig. 3). As the number of cycles increased, the curves showed a significant hysteresis due to the energy dissipation caused by internal friction in SMPLA, Mag-SMPLA, and Lig-SMPLA. At 55 °C, the hysteresis of SMP was more obvious than that at 45 °C, which may be because the internal motion of the material increased as the temperature increased, thus the energy dissipation caused by friction also increased. The first loading-unloading cycle exhibited the greatest energy dissipation, probably because microcracks started to develop. After ten load-unload cycles, the energy dissipation gradually stabilized.

When SMPLA, Mag-SMPLA, and Lig-SMPLA were combined as functional multi-responsive SMP composites, the bond strength was critical as it determined the overall mechanical properties. Therefore, standard specimens for tensile testing were prepared by combining SMPLA, Mag-SMPLA, and Lig-SMPLA in pairs to precisely assess the stress-strain behavior of the multi-responsive SMP composites. SMPLA + Mag SMPLA, SMPLA + Lig-SMPLA, and Mag SMPLA + Lig-SMPLA showed excellent and similar mechanical properties (Fig. 4a), with strengths of 34.56 MPa, 37.25 MPa, and 36.37 MPa for the three, respectively (Fig. 4b). The fracture location of SMPLA + Mag-SMPLA was exactly at the junction of the dual materials. SMPLA + Lig-SMPLA and Mag-SMPLA + Lig-SMPLA were fractured on the side close to the Lig-SMPLA part, probably due to the lower strength of Lig-SMPLA compared to SMPLA and Mag-SMPLA. In addition, the strengths of the dual-material specimens were compared with those of the single-material specimens (Fig. 4c). The largest difference was found between SMPLA + Mag-SMPLA and SMPLA, but the former strength also exceeded 75 % of the latter strength. The smallest difference was found between SMPLA + Lig-SMPLA and Lig-SMPLA, with the former strength exceeding 98 % of the latter strength.

2.2. *Precisely controllable actuation*

Light-responsive SMPLA combined with 4D printing enables configuration transformation with precise control of time and space. The shape recovery process of the 4D printed Lig-SMPLA complex configurations is shown in Figs. 5 and 6, showing high printing accuracy and

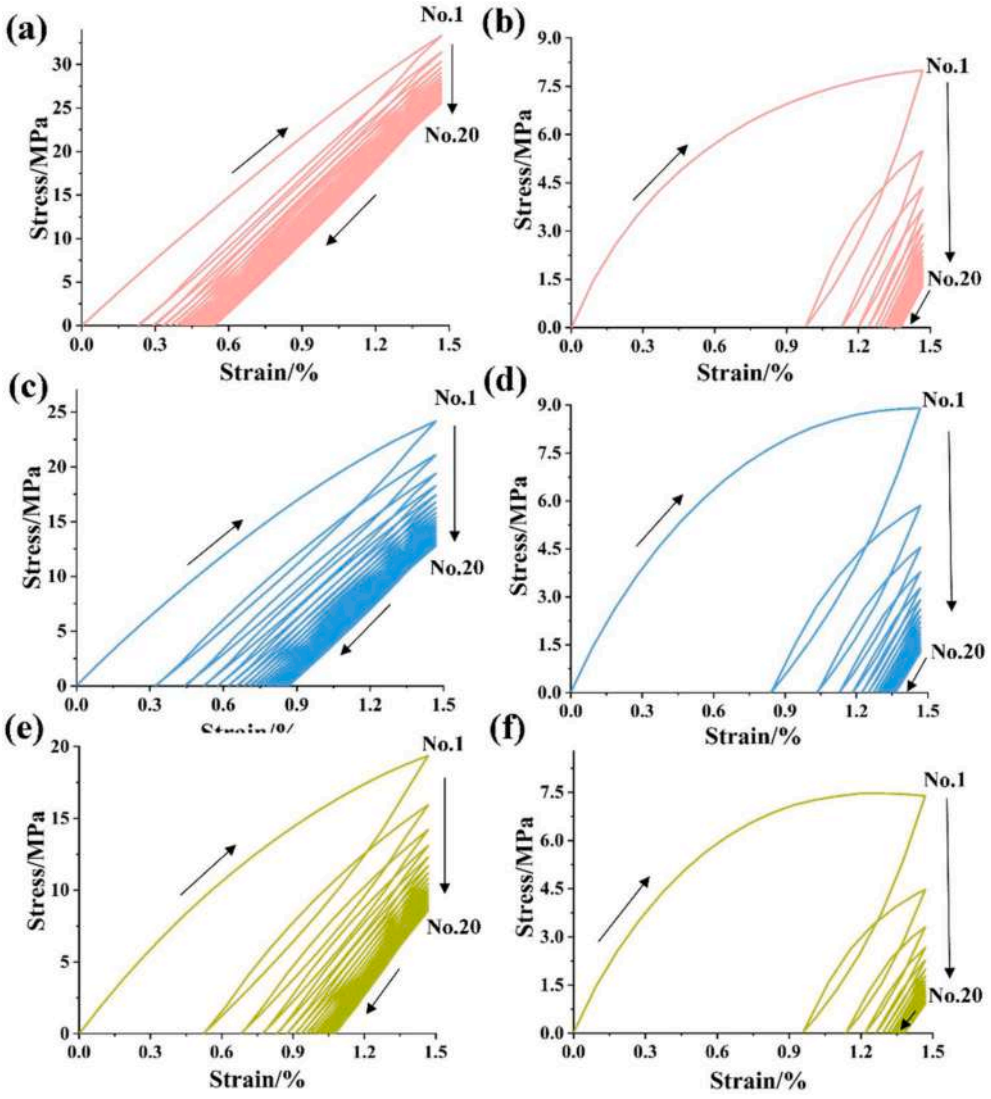

Fig. 3. Tensile stress-strain behavior of SMPLA, Mag-SMPLA, and Lig-SMPLA with 20 cycles of loading and unloading. (a) SMPLA, 45 °C, (b) SMPLA, 55 °C. (c) Mag-SMPLA, 45 °C, (d) Mag-SMPLA, 55 °C. (e) Lig-SMPLA, 45 °C, (f) Lig-SMPLA, 55 °C.

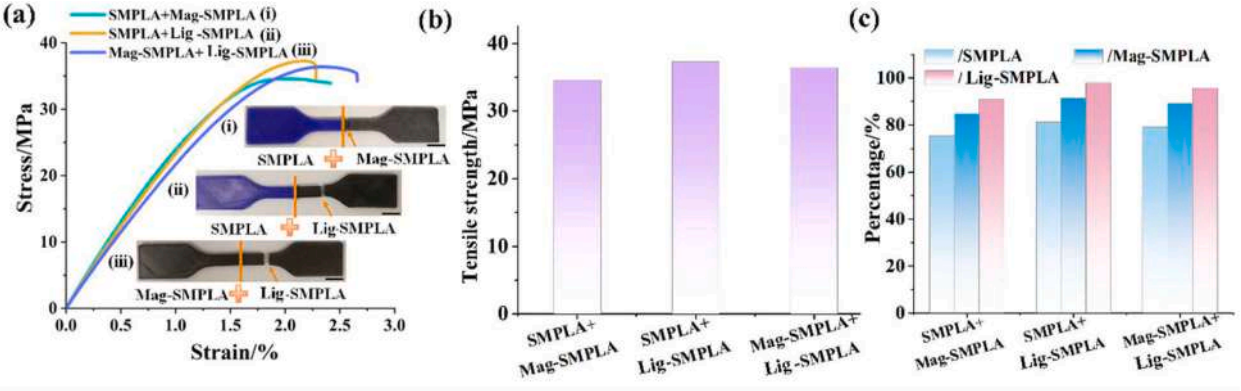

Fig. 4. Mechanical behaviors of SMPLA + Mag-SMPLA, SMPLA + Lig-SMPLA, and Mag-SMPLA + Lig-SMPLA. (a) Stress-strain curves at room temperature. (b) Tensile strength. (c) Percentage of dual-material specimen strength to single-material specimen strength. "/SMPLA" = dual-material specimen strength/SMPLA strength × 100 %; "/Mag-SMPLA" = dual-material specimen strength/Mag-SMPLA strength × 100 %; "/Lig-SMPLA" = dual-material specimen strength/Lig-SMPLA strength × 100 %.

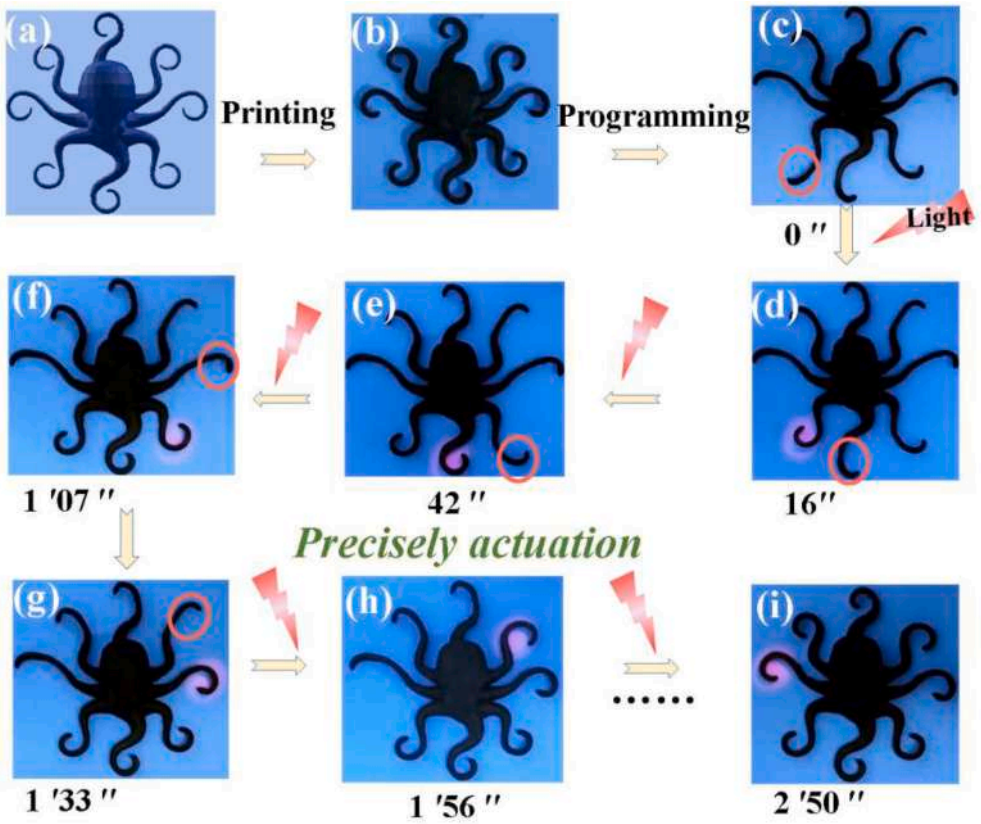

Fig. 5. 4D printed light-responsive octopus (a) 3D model. (b) 4D printed octopus. (c) Temporary configuration of the octopus. (c-i) Precisely controlled light-responsive shape recovery process. (i) 4D printed octopus after shape recovery.

excellent printing performance (Video S1, Fig. S2). Fig. 5c shows the programmed temporary configuration with the eight curled tentacles of the octopus opened. By manipulating the irradiation position and irradiation time of the light, the recovery of the tiny antennae and the sequence of their recovery were precisely controlled (Fig. 5c–i). Similarly, the wings of eagles were assigned as folded temporary configurations (Fig. 6). The control of the wing angle can be achieved by controlling the irradiation time and position of the laser during the recovery process. The folded eagle wings were able to return to the unfolded state, showing outstanding light-responsive shape memory performance. It only took 2 min 50 s to complete the shape recovery of the eight tentacles of the octopus and 1 min 11 s to complete the shape recovery of the wings of the owl. Under light stimulation, the printed complex configurations underwent progressive and targeted configuration changes, exhibiting precise and convenient controllability.

Supplementary video related to this article can be found at https://doi.org/10.1016/j.compositesb.2024.111257

2.3. Multi-responsive actuation

The multi-responsive SMP composites were obtained by combining Lig-SMPLA (I), SMPLA (II), and Mag-SMPLA (III) (Fig. 7). The straight multi-responsive SMP composite (configuration 1) was programmed into a heart-shaped temporary configuration (configuration 2). First, an alternating magnetic field was applied to the Mag-SMPLA module, which underwent shape recovery in response to the magnetic field to obtain configuration 3. Then the SMPLA module was thermally stimulated and configuration 4 was obtained. Finally, the Lig-SMPLA module was exposed to light, and the Lig-SMPLA module recovered to its initial configuration. The multi-responsive SMP composite re-exhibited its configuration 1. Therefore, the SMP composite showed a quadruple shape memory effect (configuration 1-4), with three programmed temporary configurations (configuration 2-4).

2.4. Applications

The 4D printed multi-responsive SMP composites achieved highly controllable programming and deformation, demonstrating attractive application potential in complex precision devices requiring multiple tunable configurations. This section showed the broad application prospects of the multi-responsive SMP composites with examples of robotic hands, highly programmable metamaterials, and encrypted information carriers.

2.4.1. Robotic hands

Robotic hands are of great importance in practical engineering as they can greatly save manpower and improve efficiency, and are especially important for work scenarios with high-risk factors. The application of the 4D printed multi-responsive SMP composites as robotic hands was demonstrated, which can complete the entire process of lifting and releasing objects. The working principle of the SMP robotic hands to lift/release objects is shown in Fig. 8. The Lig-SMPLA and the SMPLA were combined to obtain a linear-shaped multi-responsive SMP composite (Fig. 8a). The composite was programmed as two S-shaped robotic hands with left and right symmetry (Fig. 8b). The SMPLA modules of the robotic hands were first thermally stimulated and automatically returned to a “hook” shape (Fig. 8c and d), which can lift the object (Fig. 8d). Then the Lig-SMPLA modules of the robotic hands were then stimulated with light, and the robotic hands recovered to their initial linear shape, which can complete the release of the object (Fig. 8e and f).

Fig. 9 and Video S2 show the SMP robotic hands lifting and releasing a basket containing a full can of cola, clips, glue sticks, etc. (≈350 g) to simulate the loading/unloading of baskets with various goods in practical applications. Fig. 9a1 shows two symmetrical S-shaped robotic

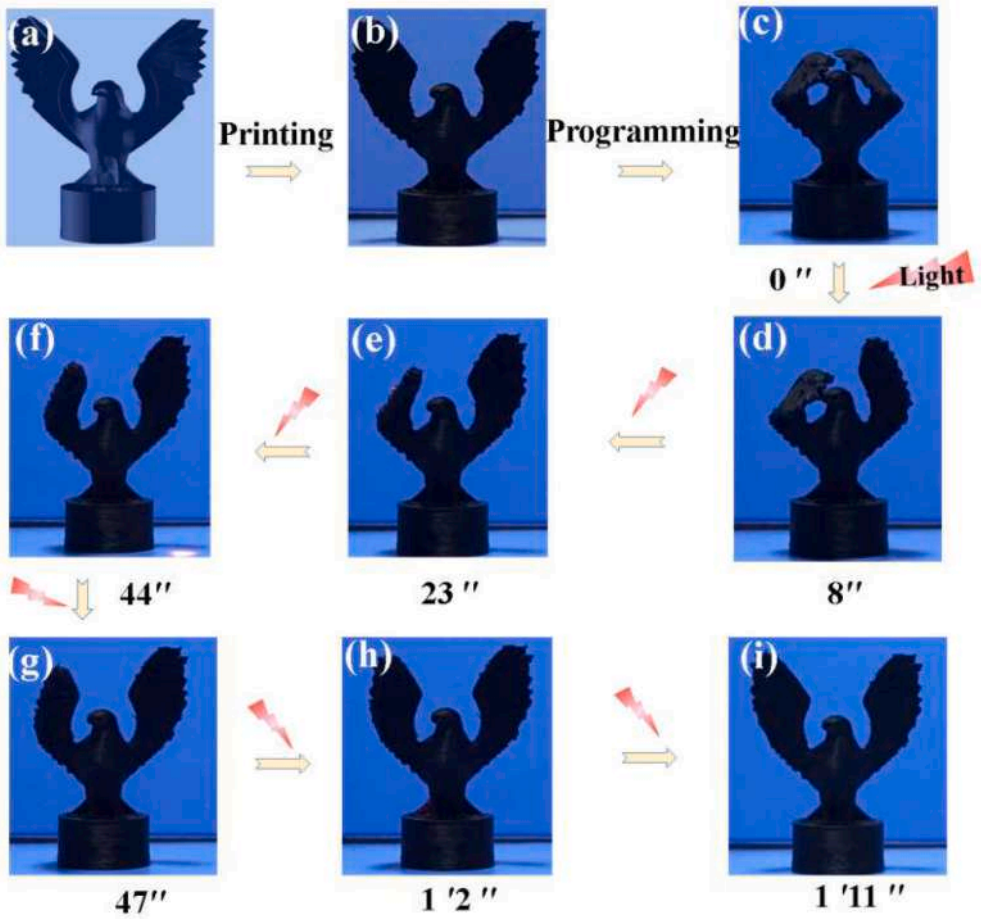

Fig. 6. 4D printed light-responsive eagle (a) 3D model. (b) 4D printed eagle. (c) Temporary configuration of the eagle. (c-i) Light-responsive shape recovery process. (i) 4D printed eagle after shape recovery.

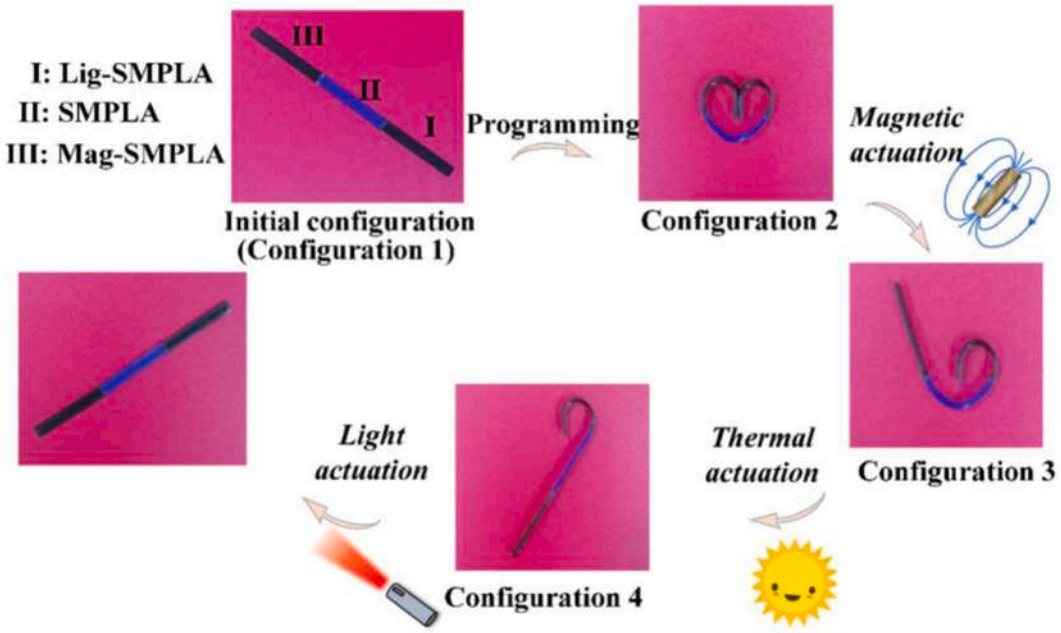

Fig. 7. Selectively programmable multi-responsive shape memory process. The Lig-SMPLA (I), SMPLA (II), and Mag-SMPLA (III) composites showed a quadruple shape memory effect.

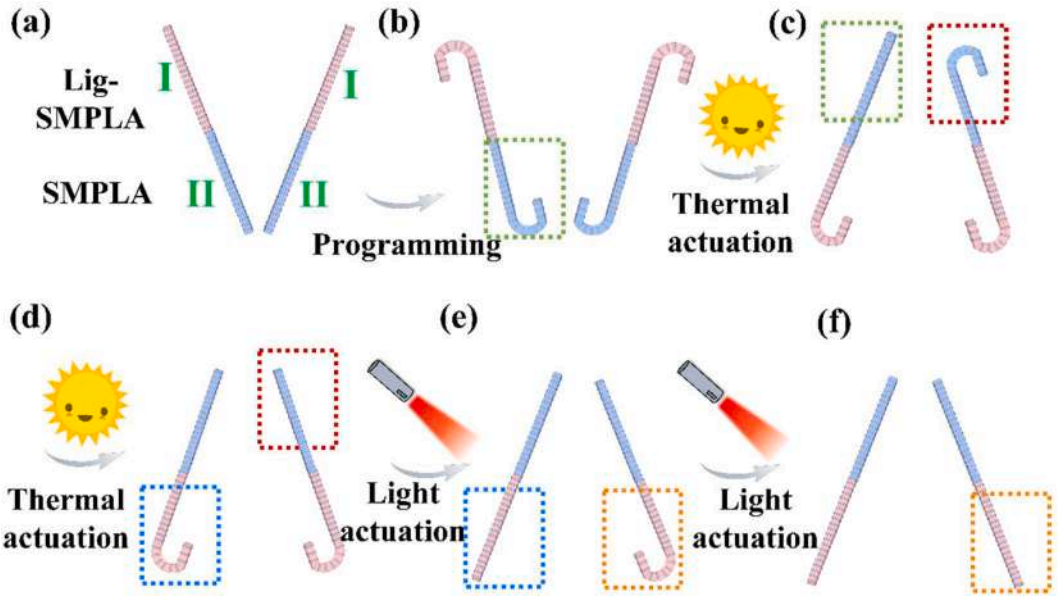

Fig. 8. Working principle of the 4D printed Lig-SMPLA + SMPLA composites as robotic hands to lift and release objects.

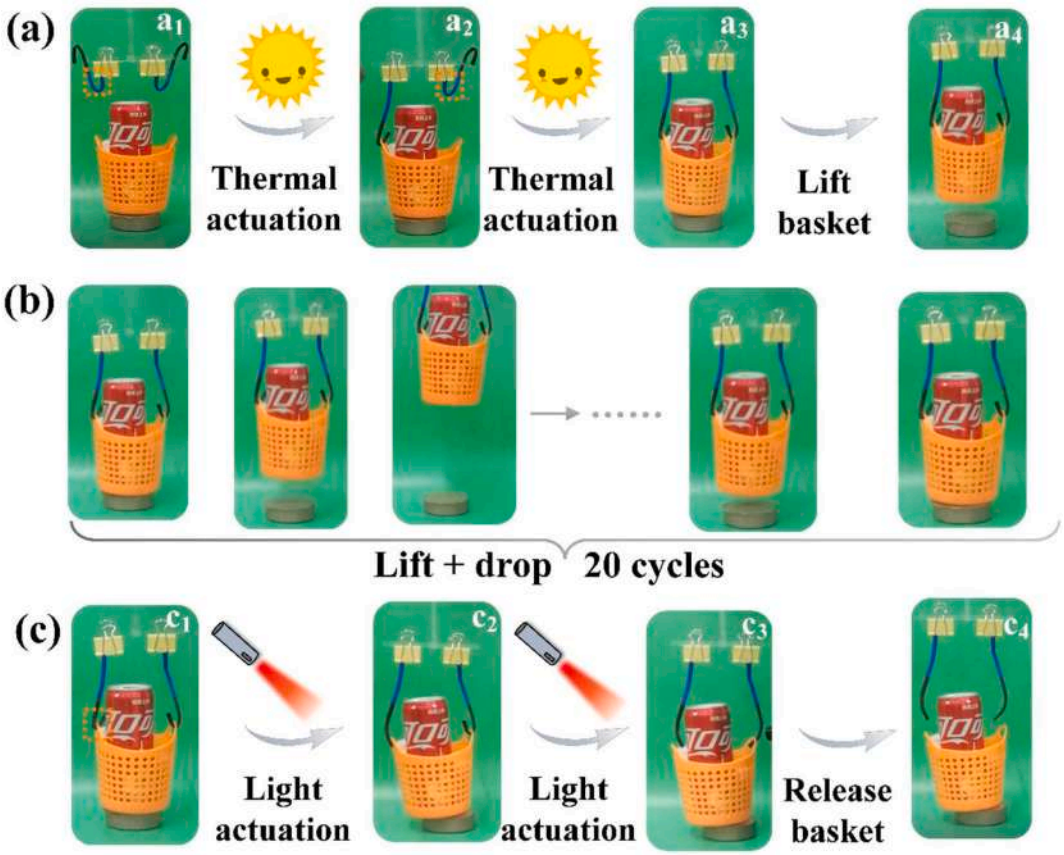

Fig. 9. The robotic hands lifted and released the basket. (a) The SMPLA modules of the robotic hands underwent shape recovery and the basket was lifted. (b) The robotic hands can lift and drop the basket (containing a full can of cola, clips, glue sticks, etc.) 20 times without damage. (c) The Lig-SMPLA modules of the robotic hands underwent shape recovery and the basket was released.

hands in a temporary configuration after programming. First, the SMPLA modules of the left and right robotic hands were actuated under thermal stimulation (Fig. 9a2, 9a3). The downward recovery deformation of the robotic hands realized the lifting of the basket (Fig. 9a4), showing excellent mechanical properties. At this time, the Lig-SMPLA modules as load-bearing modules were still in the temporary configuration without deformation, demonstrating excellent shape fixation performance. The robotic hands can lift and drop the basket for 20 cycles without any damage, further demonstrating the outstanding mechanical properties and shape memory performance (Fig. 9b, Video S2). Then,

the robotic hands were exposed to light, and the Lig-SMPLA modules underwent shape recovery, completing the basket release (Fig. 9c). The stability of the robotic hands during lifting and releasing was sufficient to keep the balance of the basket, thus ensuring that various goods loaded in the container can be transported intact in practical applications.

Supplementary video related to this article can be found at https://doi.org/10.1016/j.compositesb.2024.111257

2.4.2. Encrypted information carrier

In the current fast-moving digital era, information security is extremely critical for various departments and institutions and has a significant impact on economic development [30,31]. Therefore, it is of great importance to break the limitation of traditional manufacturing technology on the complexity of information codes and to manufacture novel information carriers for texts and images in a fast and efficient manner. A novel information carrier with a reliable encryption strategy, facile manufacturing process, and the ability to deliver diverse information was developed using the 4D printed multi-responsive SMP composites. Different from the traditional binary codes and Morse codes, the 4D printed multi-responsive SMP composites guaranteed the possibility of preparing complex configurations with high reproducibility. More importantly, it enabled the encrypted transmission of not only text information but also image information.

The schematic of the 4D printed multi-responsive SMP composite as an information carrier for encryption and decryption is shown in Fig. 10. The 4D printed SMP information carrier consisted of three modules fabricated by Lig-SMPLA, SMPLA, and Mag-SMPLA. Fig. 10a shows the initial configuration of the multi-responsive SMP information carrier. By programming, the temporary configuration was displayed (Fig. 10b) and the initial configuration was hidden, thus enabling the encryption of information. When decryption was required, the SMP information carrier was selectively actuated by light, thermal, and magnetic field, respectively. The three modules in the temporary configuration sequentially recovered to the initial configuration, and the information decryption was achieved (Fig. 10b–e). Through selective actuation, the composite can exhibit eight different configurations (multi-shapes), achieving eight shape memory effects (Fig. 11).

Fig. 12 shows the physical images of the multi-responsive SMP information carrier and its encryption and decryption process. Two text messages "10000" and "Gallop" were included in the Lig-SMPLA module, while one image message "Horse" was included in the SMPLA module (Fig. 12a). After programming, only the cluttered square blocks were presented on the temporarily configured SMP information carrier and the text/image information was hidden (Fig. 12b). The decryption process was as follows (Fig. 12c–e): first, the encrypted "10000" Lig-SMPLA module was selectively actuated by light to recover to the initial configuration, and "10000" was displayed again. Then, the encrypted "Horse" SMPLA module was selectively actuated by a heat gun, and the disorganized temporary configuration recovered to the initial "Horse" configuration. Finally, the encrypted "Gallop" Mag-SMPLA module was selectively actuated by the magnetic field, and the "Gallop" information was released. The decryption was completed, and the recovered configuration was highly consistent with the initial configuration, proving the outstanding shape recovery performance. The three modules not only represented their respective information, but also, interestingly, as a whole, they represented a Chinese idiom - "tens of thousands of Horses galloping", which meant thousands of Horses were running and leaping (Fig. S4). It can also be extended to describe mass activities with great momentum or enthusiastic scenes. The selectively programmable actuation and the excellent shape memory performance of the 4D printed multi-responsive SMP composites ensured the transmission accuracy and communication security of encrypted text and image information.

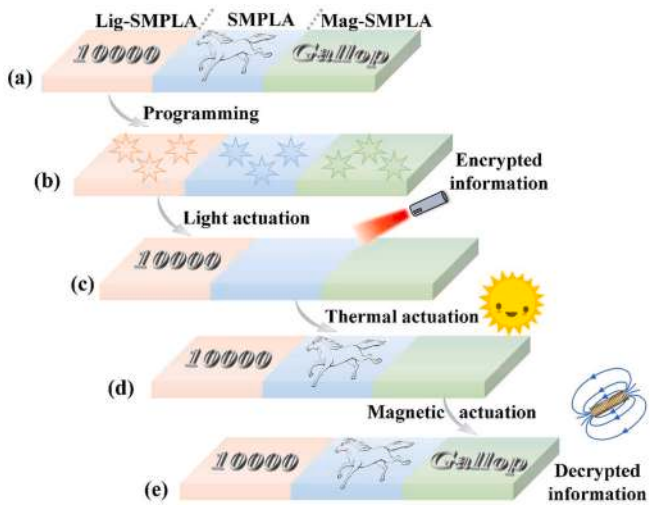

Fig. 10. Schematic of the 4D printed multi-responsive SMP composites as the information carrier.

2.4.3. Highly programmable metamaterials

Metamaterials are a class of artificial materials that can exhibit unique properties that natural materials do not possess. The delicate design of microstructural units and periodic arrangements of metamaterials enables the customization of mechanical properties, allowing them to demonstrate extraordinary potential for applications in aerospace, biomedical, and other fields [32–36]. The combination of SMPs and metamaterials enables the programmability of metamaterials in terms of structure and properties, but their programmability is limited by the singularity of material responsiveness and actuation methods. Fortunately, introducing multi-responsive SMPs into metamaterials combined with region-selective actuation can greatly improve metamaterials' designability and programming freedom.

Fig. 13a shows the designed metamaterial structure and geometric parameters. The metamaterial unit cell consists of a central circular node and four arc-shaped ligaments, where $r/R = 0.429$, $w/R = 0.571$, $t/R = 0.571$, and $\alpha = \pi$. Fig. 13b–d shows the structures and stress-strain curves of permanent and programmed temporary configurations of SMPLA, Mag-SMPLA, and Lig-SMPLA metamaterials. The tensile strengths of SMPLA PC and SMPLA TC were 1.19 MPa and 2.43 MPa, respectively, and the elongations at break were 51.1 % and 13.2 %, respectively. The low strength and high elongation at break of SMPLA PC were closely related to the metamaterial ligament structure. The arc-shaped ligaments were gradually straightened during the stretching process, and the deformation mode was a combination of bending dominance and stretching dominance. In contrast, the ligaments of the programmed SMPLA TC were almost straight, and the straight ligaments were directly stretched with little bending deformation as a cushion, leading to increased strength and decreased elongation at break. The stress-strain curves of Mag-SMPLA metamaterials and Lig-SMPLA metamaterials before and after programming showed similar trends. The strength of Mag-SMPLA TC (Mag TC) was slightly higher than that of Lig-SMPLA TC (Lig TC), which were 2.32 MPa and 2.15 MPa, respectively.

By preparing multi-responsive SMP composites, the programmability of metamaterials can be tripled (from one temporary configuration to three temporary configurations). Fig. 13e shows the Mag-SMPLA + Lig-SMPLA metamaterial, where two additional programmed temporary configurations (Mag PC + Lig TC and Mag TC + Lig PC) can be obtained by selective actuation. Both Mag PC + Lig TC and Mag TC + Lig PC were a combination of straight ligaments and curved ligaments, thus their mechanical behaviors were between those of Mag PC + Lig PC and Mag TC + Lig TC. In the multi-responsive SMP composite, the component in temporary configuration was the main determinant of the overall strength of the module. The strength of Mag TC was higher than that of

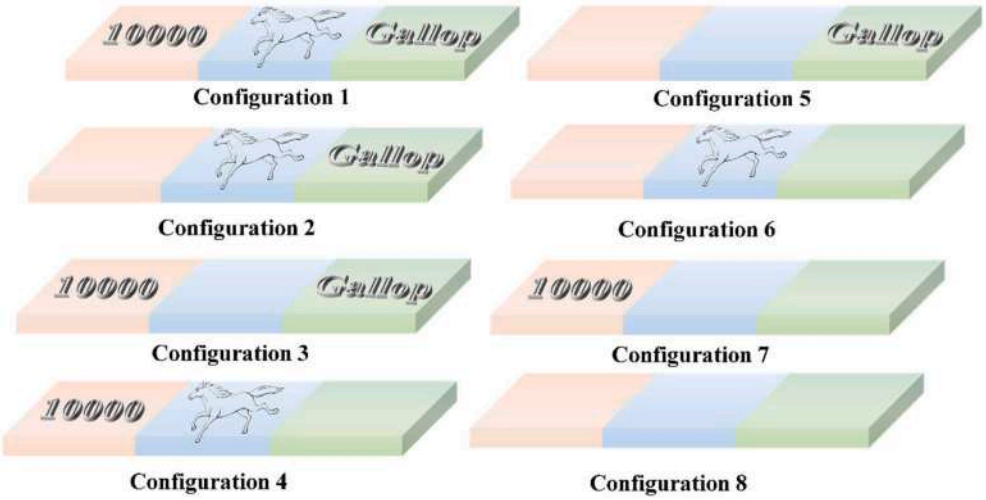

Fig. 11. Eight configurations of 4D printed multi-responsive SMP composites. Configuration 1 represents all information displayed, and configuration 8 represents all information encrypted.

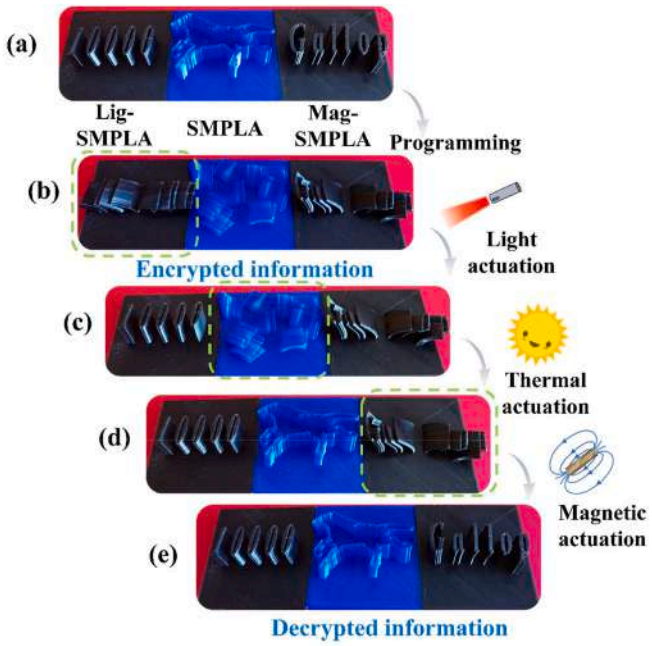

Fig. 12. Physical images of the 4D printed multi-responsive SMP composites information carrier and its encryption and decryption process. (a) Initial configuration, (b) temporary configuration, and (c-e) decryption process of the 4D printed multi-responsive SMP information carrier.

Lig TC, and accordingly, the strength of Mag TC + Lig PC was also higher than that of Mag PC + Lig TC. Similarly, the SMPLA and Mag-SMPLA composite exhibited three programmed temporary configurations (Fig. 13f). SMPLA TC + Mag TC had the highest strength and lowest elongation at break; SMPLA PC + Mag PC had the lowest strength and highest elongation at break; SMPLA PC + Mag TC and SMPLA TC + Mag PC had intermediate strength and elongation at break. Fig. S3 and Video S3 show the deformation process of the 4D printed multi-responsive SMP metamaterials.

Supplementary video related to this article can be found at https://doi.org/10.1016/j.compositesb.2024.111257

Fig. 14a shows the 4D printed Mag PC + Lig PC metamaterials, and Mag TC + Lig TC metamaterials were obtained after programming Mag PC + Lig PC metamaterials (Fig. 14b). The selective actuation of the 4D printed Mag TC + Lig TC was demonstrated (Fig. 14c, Video S4). In an alternating magnetic field, the Mag TC module was selectively actuated and the ligaments recovered from the straight configuration to the initial curved configuration (Mag PC + Lig TC). While the Lig TC module cannot be actuated in the magnetic field and the ligaments remained in the temporary configuration. When exposed to light, the Lig TC module was actuated and the Mag PC + Lig PC metamaterial was finally obtained.

Supplementary video related to this article can be found at https://doi.org/10.1016/j.compositesb.2024.111257

Therefore, by combining multi-responsive SMPs with selective actuation, the programmability of metamaterials can be tripled, thus greatly improving the design freedom and utilization of metamaterial devices. The introduction of highly programmable metamaterials into engineering applications will yield significant economic benefits, allowing for multiple uses of a single device, and thereby significantly reducing production costs.

3. Conclusion

Thermal-, magnetic, and light-responsive 4D printed SMP composites with up to eight shape memory effects were fabricated in a facile way, which can be adapted to applications requiring more tunable configurations, greatly broadening the application range of SMP. Notably, the design and fabrication strategy for 4D printed multi-shape SMP circumvented the barriers to mass production, representing a meaningful step in closing the gap between modeling and engineering applications of 4D printed multi-shape SMP intelligent devices.

The 4D printed multi-responsive SMP composites demonstrated attractive application potential in flexible robotics, highly programmable metamaterials, and encrypted information carriers. The multi-responsive SMP robotic hands were able to lift and drop baskets loaded with various goods 20 times without damage. The programmability of 4D printed multi-responsive SMP metamaterials can be tripled, significantly improving the design freedom and utilization of metamaterial devices. In addition, 4D printed multi-responsive SMP information carriers broke the limitation of traditional manufacturing technology on the complexity of information encoding and realized efficient encrypted transmission not only of text information but also of image information. Due to the advantages of selective programming, highly controllable deformation, and customized configuration, the application prospects of multi-responsive SMP composites are not limited to the above applications, but also have broad application prospects in electronic sensing, self-assembled structures, aerospace,

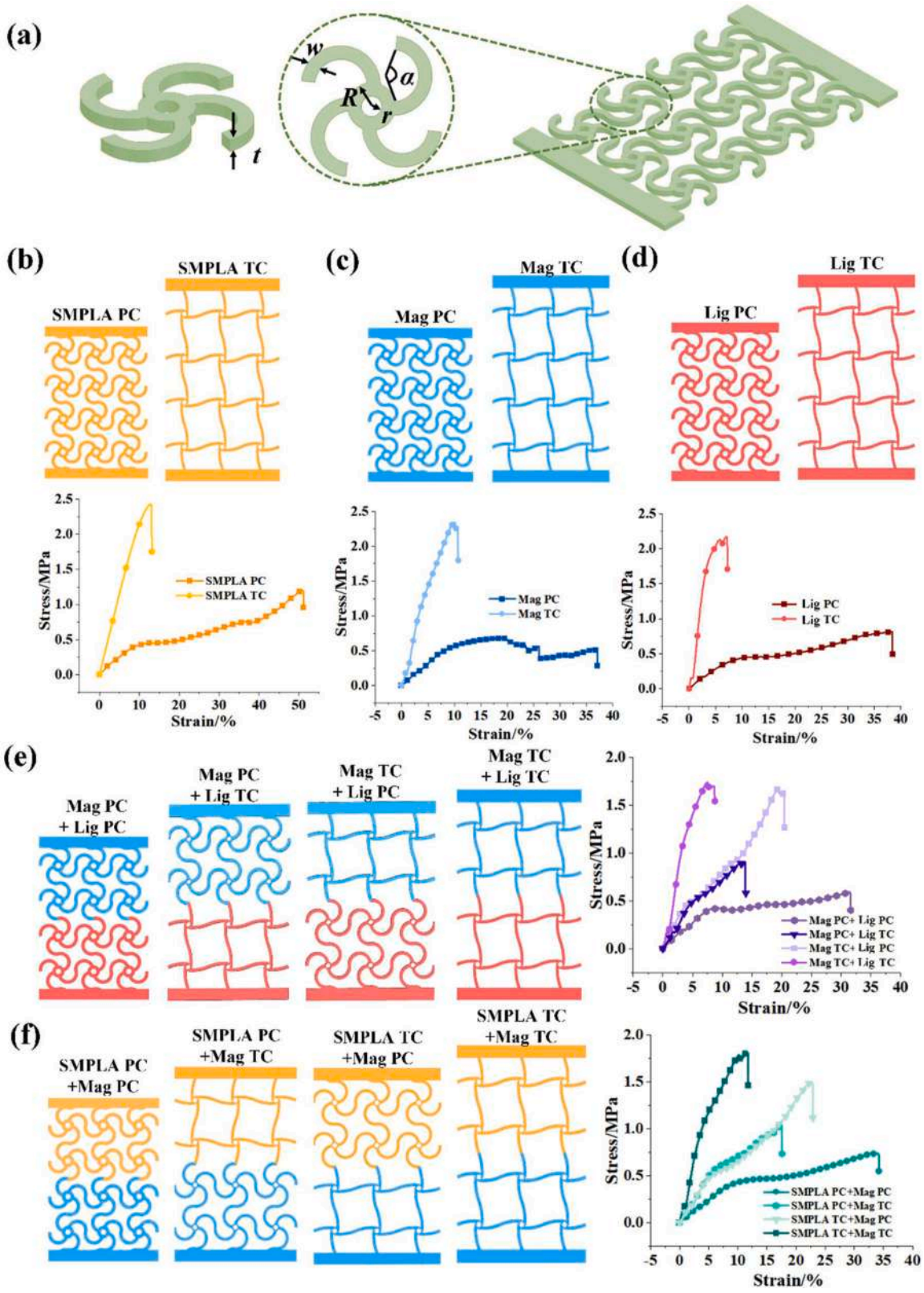

Fig. 13. (a) Design and geometric parameters of metamaterials. (b) Structures and stress-strain curves of permanent and programmed temporary configurations (1 temporary configuration) of SMPLA metamaterials. (c) Structures and stress-strain curves of permanent and programmed temporary configurations (1 temporary configuration) of Mag-SMPLA metamaterials. (d) Structures and stress-strain curves of permanent and programmed temporary configurations (1 temporary configuration) of Lig-SMPLA metamaterials. (e) Structures and stress-strain curves of permanent and programmed temporary configurations (3 temporary configurations) of the Mag-SMPLA + Lig-SMPLA metamaterial. (f) Structures and stress-strain curves of permanent and programmed temporary configurations (3 temporary configurations) of the SMPLA + Mag-SMPLA metamaterial. PC: permanent configuration; TC: temporary configuration. Mag-SMPLA TC: Mag TC; Lig-SMPLA TC: Lig TC.

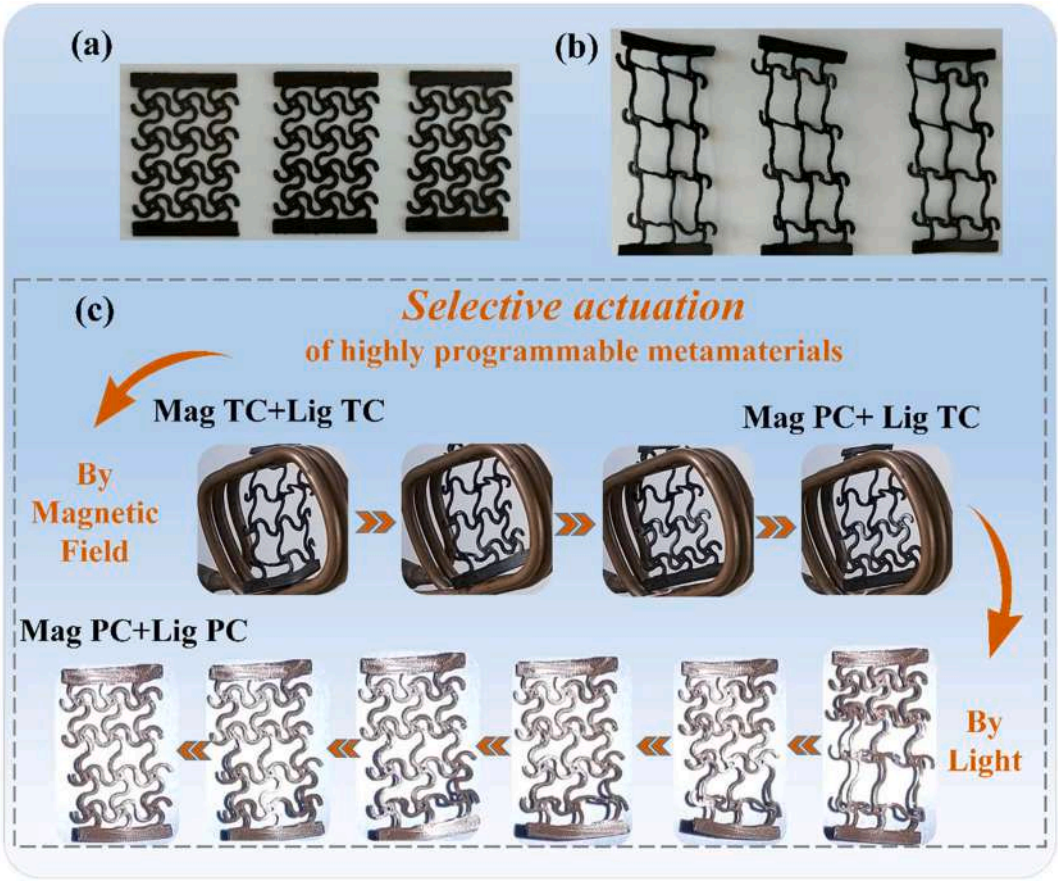

Fig. 14. (a) 4D printed Mag PC + Lig PC metamaterials. (b) 4D printed Mag TC + Lig TC metamaterials. (c) Selective actuation of 4D printed Mag TC + Lig TC metamaterials under magnetic field and light.

etc.

CRediT authorship contribution statement

Cheng Lin: Investigation, Methodology, Writing – original draft, Writing – review & editing. **Xiaozhou Xin:** Investigation, Methodology. **Linfeng Tian:** Investigation. **Dou Zhang:** Writing – review & editing. **Liwu Liu:** Investigation. **Yanju Liu:** Project administration, Supervision. **Jinsong Leng:** Supervision, Writing – review & editing.

Declaration of competing interest

The authors declare that they have no known competing financial interests or personal relationships that could have appeared to influence the work reported in this paper.

Data availability

Data will be made available on request.

Acknowledgments

This work was funded by the Interdisciplinary Research Foundation of HIT, the National Natural Science Foundation of China (Grant Nos. 12302198), and Key R&D Program of Ningbo City (2023Z191). The project was also supported by the National Key R&D Program of China (2022YFB3805700).

Appendix A. Supplementary data

Supplementary data to this article can be found online at https://doi.org/10.1016/j.compositesb.2024.111257.

References

[1] Xia Y, He Y, Zhang F, Liu Y, Leng J. A review of shape memory polymers and composites: mechanisms, materials, and applications. Adv Mater 2020:2000713.
[2] Yang S, He Y, Leng J. Shape memory poly (ether ether ketone)s with tunable chain stiffness, mechanical strength and high transition temperatures. Int J Smart Nano Mater 2022;13(1):1–16.
[3] Lin C, Lv J, Li Y, Zhang F, Li J, Liu Y, Liu L, Leng J. 4D-Printed biodegradable and remotely controllable shape memory occlusion devices. Adv Funct Mater 2019: 1906569.
[4] Biswas MC, Chakraborty S, Bhattacharjee A, Mohammed Z. 4D printing of shape memory materials for textiles: mechanism, mathematical modeling, and challenges. Adv Funct Mater 2021:31.
[5] Lin C, Liu L, Liu Y, Leng J. Recent developments in next-generation occlusion devices. Acta Biomater 2021;128:100–19.
[6] Zhang B, Li HG, Cheng JX, Ye HT, Sakhaei AH, Yuan C, Rao P, Zhang YF, Chen Z, Wang R, He XN, Liu J, Xiao R, Qu SX, Ge Q. Mechanically robust and UV-curable shape-memory polymers for digital light processing based 4D printing. Adv Mater 2021:33.
[7] Sabzi M, Babaahmadi M, Rahnama M. Thermally and electrically triggered triple-shape memory behavior of poly(vinyl acetate)/Poly(lactic acid) due to graphene-induced phase separation. ACS Appl Mater Interfaces 2017;9:24061–70.
[8] Zhang F, Wen N, Wang L, Bai Y, Leng J. Design of 4D printed shape-changing tracheal stent and remote controlling actuation. Int. J. Smart Nano Mater. 2021;12: 375–89.
[9] Kim JC, Chang YW, Sabzi M. Designing self-crosslinkable ternary blends using epoxidized natural rubber (ENR)/poly(ethylene-co-acrylic acid)(EAA)/poly (epsilon-caprolactone) (PCL) demonstrating triple-shape memory behavior. Eur Polym J 2021:152.
[10] Shi GQ, Huang C, Cao XY, Liu MY, Zhang JN, Zheng K, Ma YM. Triple shape memory effect of ethylene-vinyl acetate copolymer/poly (propylene carbonate) blends with broad composite ratios and phase morphologies. Polymer 2021:231.

[11] Curtis SM, Sielenkämper M, Arivanandhan G, Dengiz D, Li ZX, Jetter J, Hanke L, Bumke L, Quandt E, Wulfinghoff S, Kohl M. TiNiHf/SiO2/Si shape memory film composites for bi-directional micro actuation. Int. J. Smart Nano Mater. 2022;13:293–314.
[12] Zhao F, Zheng X, Zhou S, Zhou B, Xue S, Zhang Y. Constitutive model for epoxy shape memory polymer with regulable phase transition temperature. Int J Smart Nano Mater 2021;12(1):72–87.
[13] Gu J, Zhang X, Duan H, Wan M, Sun H. A hygro-thermo-mechanical constitutive model for shape memory polymers filled with nano-carbon powder. Int J Smart Nano Mater 2021;12(3):286–306.
[14] Lin C, Huang Z, Wang Q, Wang W, Wang W, Wang Z, Liu L, Liu Y, Leng J. 3D printed bioinspired stents with photothermal effects for malignant colorectal obstruction. Research 2022:1–12.
[15] Pei M, Hwangbo H, Kim G. Hierarchical fibrous collagen/poly(ε-caprolactone) structure fabricated with a 3D-printing process for tissue engineering applications. Compos B Eng 2023;259:110730.
[16] Huang Y, Tian X, Li W, He S, Zhao P, Hu H, et al. 3D printing of topologically optimized wing spar with continuous carbon fiber reinforced composites. Compos B Eng 2024;272:111166.
[17] Geng Y, Liu T, Zhao M, Wei H, Yao X, Zhang Y. Silk fibroin/polyacrylamide-based tough 3D printing scaffold with strain sensing ability and chondrogenic activity. Compos B Eng 2024;271:111173.
[18] Wu T, Lu Y, Yang X, Liu D, Ji Z, Wang X, et al. Vat photopolymerization 3D printing of oil filled cyanate ester for one-step fabricating self-lubricating parts. Compos B Eng 2023;266:110996.
[19] Zhang Y, Raza A, Xue Y, Yang G, Hayat U, Yu J, Liu C, Wang H, Wang J. Water-responsive 4D printing based on self-assembly of hydrophobic protein "Zein" for the control of degradation rate and drug release. Bioact Mater 2023;23:343–52.
[20] Lin C, Liu L, Liu Y, Leng J. 4D printing of shape memory polybutylene succinate/polylactic acid (PBS/PLA) and its potential applications. Compos Struct 2022;279:114729.
[21] Mahmood A, Akram T, Shenggui C, Chen H. Revolutionizing manufacturing: a review of 4D printing materials, stimuli, and cutting-edge applications. Compos B Eng 2023;266:110952.
[22] Ren L, Wang Z, Ren L, Xu C, Li B, Shi Y, et al. Understanding the role of process parameters in 4D printing: a review. Compos B Eng 2023;265:110938.
[23] Ren L, Wang Z, Ren L, Han Z, Zhou XL, Song Z, et al. 4D printing of shape-adaptive tactile sensor with tunable sensing characteristics. Compos B Eng 2023;265:110959.
[24] Zhou X, Ren L, Song Z, Li G, Zhang J, Li B, et al. Advances in 3D/4D printing of mechanical metamaterials: from manufacturing to applications. Compos B Eng 2023;254:110585.
[25] Wang Y, Cui HT, Esworthy T, Mei DQ, Wang YC, Zhang LG. Emerging 4D printing strategies for next-generation tissue regeneration and medical devices. Adv Mater 2022:34.
[26] Fu P, Li HM, Gong J, Fan ZJ, Smith AT, Shen KY, Khalfalla TO, Huang HF, Qian X, McCutcheon JR, Sun LY. 4D printing of polymers: techniques, materials, and prospects. Prog Polym Sci 2022:126.
[27] Guan ZC, Wang L, Bae J. Advances in 4D printing of liquid crystalline elastomers: materials, techniques, and applications. Mater Horiz 2022;9:1825–49.
[28] Lin C, Zhang L, Liu Y, Liu L, Leng J. 4D printing of personalized shape memory polymer vascular stents with negative Poisson's ratio structure: a preliminary study. Sci China Technol Sci 2020;63:578–88.
[29] Zhao Q, Li C, Shum HC, Du X. Shape-adaptable biodevices for wearable and implantable applications. Lab Chip 2020;20:4321–41.
[30] Ma QQ, Wang J, Li ZH, Wang D, Hu XX, Xu YS, Yuan Q. Near-infrared-light-mediated high-throughput information encryption based on the inkjet printing of upconversion nanoparticles. Inorg Chem Front 2017;4:1166–72.
[31] Xiao Q, Ma Q, Yan T, Wu LW, Liu C, Wang ZX, Wan X, Cheng Q, Cui TJ. Orbital-angular-momentum-encrypted holography based on coding information metasurface. Adv Opt Mater 2021:9.
[32] Xin XZ, Liu LW, Liu YJ, Leng JS. 4D pixel mechanical metamaterials with programmable and reconfigurable properties. Adv Funct Mater 2022:32.
[33] Wu WW, Kim S, Ramazani A, Cho YT. Twin mechanical metamaterials inspired by nano-twin metals: experimental investigations. Compos Struct 2022:291.
[34] Lin C, Liu L, Liu Y, Leng J. 4D printing of bioinspired absorbable left atrial appendage occluders: a proof-of-concept study. ACS Appl Mater Interfaces 2021;13:12668–78.
[36] Xin XZ, Liu LW, Liu YJ, Leng JS. 4D printing auxetic metamaterials with tunable, programmable, and reconfigurable mechanical properties. Adv Funct Mater 2020:30.
[35] Qi JX, Chen ZH, Jiang P, Hu WX, Wang YH, Zhao Z, Cao XF, Zhang SS, Tao R, Li Y, Fang DI. Recent progress in active mechanical metamaterials and construction principles. Adv Sci 2022:9.